

Human scotopic sensitivity is regulated postreceptorally by changing the speed of the scotopic response

Andrew Stockman

Institute of Ophthalmology, University College London,
London, UK



Toby Candler

Institute of Ophthalmology, University College London,
London, UK



Lindsay T. Sharpe

Institute of Ophthalmology, University College London,
London, UK



Sensitivity regulation enables the visual system to function effectively from the absorption of a few photons at the lowest visual threshold to the absorption of enough photons to bleach nearly all the light-sensitive photopigment in the eye. Here, we investigate sensitivity regulation in the rod (or scotopic) range from -3.8 to $-0.8 \log_{10}$ scotopic trolands. Over most of this range, the rate of photon absorption per rod is too low for sensitivity regulation to be practicable within the rod photoreceptor itself, so that regulation must occur postreceptorally. We measured adaptation-dependent changes in visual sensitivity and visual delay, which together provide a much more complete characterization of the effects of light adaptation than the usual method of measuring sensitivity changes alone. Our results demonstrate clearly that changes in scotopic sensitivity with increasing light levels are achieved in large part by a speeding up of the scotopic response and a decrease in the temporal integration time. Thus, the scotopic and the photopic systems both regulate their steady-state sensitivity using the same strategy, even though the scotopic system does it largely postreceptorally and the photopic system largely receptorally.

Keywords: light adaptation, rods, scotopic, temporal sensitivity, phase delays, sensitivity regulation, temporal integration time

Citation: Stockman, A., Candler, T., & Sharpe, L. T. (2010). Human scotopic sensitivity is regulated postreceptorally by changing the speed of the scotopic response. *Journal of Vision*, 10(2):12, 1–19, <http://journalofvision.org/10/2/12/>, doi:10.1167/10.2.12.

Introduction

The human visual system is able to operate over a range of environmental light levels greater than $1:10^{10}$. This remarkable feat is achieved in part by dividing the range between the sensitive rod photoreceptors at low or “scotopic” levels, and the less-sensitive cone photoreceptors at high or “photopic” levels, the two working together at intermediate “mesopic” levels (Parinaud, 1881; Schultze, 1866; von Kries, 1894, 1896). In two previous papers, we have investigated steady-state cone or photopic adaptation (Stockman, Langendörfer, & Sharpe, 2007; Stockman, Langendörfer, Smithson, & Sharpe, 2006). Here, using comparable techniques, we investigate rod adaptation.

Our previous data on photopic adaptation were consistent with sensitivity being regulated by two broad classes of mechanism. The first class turns off the visual response more quickly as the light level increases, thus shortening the visual integration time. At the molecular level, this speeding up is achieved either by increasing the rates of decay or by removal of active molecules in the visual transduction cascade. At the psychophysical level, the

effects of these changes are evident as increases in the observer’s relative sensitivity to higher flicker frequencies and as reductions in perceived visual delay. The second class of mechanism scales the visual response as the light level increases. At the molecular level, this scaling is achieved by increasing the rates of molecular resynthesis and raising the sensitivity of gated ion-channels, both of which paradoxically increase sensitivity with increasing light intensity; and by the depletion of the photopigment by bleaching, which decreases sensitivity. At the psychophysical level, the effects of these changes are evident as overall (temporal-frequency-independent) increases or decreases in the observers’ sensitivity without changes in perceived visual delay. See Stockman et al. (2006, 2007) for further details of this work. For reviews and models of photoreceptor adaptation at the molecular level, see, for example, Arshavsky, Lamb, and Pugh (2002), Burns and Baylor (2001), Hamer, Nicholas, Tranchina, Lamb, and Jarvinen (2005), Pugh and Lamb (2000), and Pugh, Nikonov, and Lamb (1999), and for reviews of previous work on light adaptation, see, for example, Graham and Hood (1992), Hood (1998), Hood and Finkelstein (1986), MacLeod (1978), and Shapley and Enroth-Cugell (1984).

What mechanisms, then, are likely to regulate scotopic sensitivity? A crucial difference between scotopic and photopic sensitivity regulation is that the former operates at much lower rates of photon absorption. At the levels used in the experiments reported here, the photon absorption rate varies from as low as 0.00245 quanta absorbed per rod every second at $-3.3 \log_{10}$ scot. td (i.e., one per rod every 6.8 minutes.) to 0.775 quanta absorbed per rod every second at $-0.8 \log_{10}$ scot. td (calculated on the assumption that 1 scot. td [or $0 \log_{10}$ scot. td] at 500 nm produces 4.89 quanta absorbed $\text{rod}^{-1} \text{s}^{-1}$, see Table 2.3 of Pugh, 1988). Thus, the rate of photon absorption at lower scotopic levels is far too low to make sensitivity regulation at the rod photoreceptor practicable (e.g., Aguilar & Stiles, 1954; Baumgardt, 1949). At, for example, $-2 \log_{10}$ scot. td—roughly the middle of the range of our measurements—each rod absorbs, on average, only one photon every 20 s. Thus, for scotopic sensitivity regulation to be responsive at these levels, the regulation must occur within postreceptoral stages where the responses of rods are pooled (see Rushton, 1965).

At higher scotopic or mesopic levels, the rates of photon absorption are high enough for sensitivity regulation to be practicable within the rod photoreceptor. And, indeed, there is evidence for such regulation in human and primate rod suction electrode recordings (Baylor, Nunn, & Schnapf, 1984; Kraft, Schneeweis, & Schnapf, 1993), and in human electroretinographic (ERG) scotopic a-wave recordings (e.g., Hood & Birch, 1993; Thomas & Lamb, 1999). These effects, however, occur at light levels well above the upper limit of $-0.8 \log_{10}$ scot. td used in our measurements. Moreover, the sensitivity losses found in suction electrode and ERG recordings are much less than those found psychophysically: backgrounds that only halve the photocurrent or ERG response (e.g., Baylor et al., 1984; Hood & Birch, 1993; Kraft et al., 1993; Thomas & Lamb, 1999) reduce the observers' psychophysical sensitivity by several log units (e.g., Aguilar & Stiles, 1954; Barlow, 1957; Rushton, 1965; Sharpe, Stockman, Fach, & Markstahler, 1993). The additional losses found psychophysically must occur postreceptorally.

Psychophysical measurements, in general, support a mainly postreceptoral locus for scotopic sensitivity regulation. For example, scotopic sensitivity measured at an unbleached retinal location can be raised by bleaching adjacent areas. Estimates of the distances over which the signals from bleached areas raise sensitivity range from 5–7.5 min. of arc (Cicerone & Hayhoe, 1990) to 10 min. (MacLeod, Chen, & Crognale, 1989) to up to 30 min. (Rushton & Westheimer, 1962). Other evidence has been obtained using high spatial-frequency gratings produced by interference patterns directly on the retina, which can be used to modulate the adaptive states of adjacent photoreceptors. When cones are excited by such patterns, distortion products are seen that are consistent with adaptation occurring locally within single cones (MacLeod & He, 1993; MacLeod, Williams, & Makous, 1992).

However, when rods are similarly excited, no distortion products are seen even near rod saturating levels, which suggests that local adaptation within individual rods is insignificant (He & MacLeod, 2000).

Given that scotopic adaptation is mainly postreceptoral and photopic adaptation mainly receptor, one might imagine that the principal scotopic and photopic sensitivity regulating mechanisms could be fundamentally different. Thus, there is no a priori reason to suppose that postreceptoral rod mechanisms, like receptor cone mechanisms, should regulate their sensitivity by shortening integration time. Instead, they might regulate sensitivity simply by attenuating the scotopic response (with no speed improvements). Relevant experimental evidence on this question comes both from physiology and from psychophysics.

Much physiological evidence points to scotopic adaptation mechanisms operating within the inner retina at low scotopic light levels (e.g., Barlow & Levick, 1969; Dowling, 1967; Enroth-Cugell & Shapley, 1973; Frishman & Sieving, 1988; Naarendorp, Sato, Cajdric, & Hubbard, 2001). Recent evidence suggests that the main site of adaptation in mouse and primate is at the synapse between rod bipolars and AII amacrine cells; the changes in gain that were observed, however, were not clearly associated with changes in response kinetics (Dunn, Doan, Sampath, & Rieke, 2006; Dunn & Rieke, 2008).

Previous psychophysical evidence

Existing psychophysical evidence on the nature of the scotopic sensitivity regulating mechanisms includes measurements of rod temporal-contrast sensitivity functions (TCSFs), rod threshold-versus-intensity (TVI) curves and rod-cone phase delays.

Temporal contrast sensitivity functions (TCSFs)

With the exception of measurements by Nygaard and Frumkes (1985), TCSF measurements show little evidence over most of the scotopic range for the relative improvements in high-frequency sensitivity that are indicative of shortening integration times (Conner, 1982; Hess & Nordby, 1986; Sharpe, Stockman, & MacLeod, 1989; Smith, 1969, 1973). Changes in the shapes of rod TCSFs are found, but not until higher scotopic or mesopic levels, where the functions change from being lowpass in shape—functions that fall monotonically with increasing frequency—to being bandpass in shape—functions that peak in sensitivity at some intermediate temporal frequency and fall off in sensitivity at both lower and higher frequencies (Conner, 1982; Hess & Nordby, 1986; Sharpe et al., 1989; Smith, 1969, 1973). It has been argued that the change from lowpass to bandpass TCSF is consistent with the emergence of a spatially opponent rod surround at mesopic levels (Smith, 1973), rather than with a shortening of the

rod integration time. However, the changes that occur at these levels are further complicated by a transition between a slow and a fast rod pathway that occurs near $0.0 \log_{10}$ scot. td (e.g., Conner, 1982; Conner & MacLeod, 1977; Sharpe et al., 1989; Stockman, Sharpe, R  ther, & Nordby, 1995). In this study, we intentionally try to avoid these complexities by restricting our analysis to levels below $-0.8 \log_{10}$ scot. td.

Threshold versus intensity (TVI) curves

A more limited test for changes in temporal integration is the comparison between detection thresholds for incremental flashes of short (e.g., 10 ms) and long (e.g., 200 ms) duration as a function of background intensity (i.e., threshold-versus-intensity or TVI measurements). If temporal summation decreases with adaptation, then the sensitivity for detecting the long duration targets (the duration of which is assumed to be longer than the temporal integration time) should decline relative to the sensitivity for detecting the short duration targets (the duration of which is assumed to be always shorter than the integration time and therefore unaffected by changes in temporal integration). Consequently, if integration time decreases with background level, then the logarithmic slope of the 200-ms TVI function should be steeper than that of the 10-ms TVI function. Because no differences were found between the logarithmic slopes of such functions, Sharpe et al. (1993) concluded that there was little or no change in rod temporal integration over most of the scotopic range. [For other relevant TVI data, see, for example, Figure 1A of Lennie (1979) and Figure 3 of Stabell, Nordby, and Stabell (1987), and for further discussion see Sharpe et al. (1993).]

Phase delays

A more direct way of monitoring the speeding up of the rod response, and one that we employ here, is to measure changes in rod phase delay as a function of adaptation level. Sharpe et al. (1989) measured the rod delay relative to a cone standard in the same eye (holding the state of cone adaptation constant but varying the state of rod adaptation). They found little change in phase delay between about $-1.6 \log_{10}$ scot. td (the lowest scotopic level they used) and $-0.3 \log_{10}$ scot. td (see their Figures 6–9).

In summary, scotopic visual delays, TVI curves and the majority of TCSFs, as well as physiological data, all suggest that scotopic sensitivity regulation is mediated not by a shortening of the integration time, but by some form of response compression or sensitivity scaling that attenuates the scotopic response without changing its speed.

Here, we reinvestigate scotopic sensitivity regulation by combining measures of temporal contrast sensitivity with measures of visual delay. Unexpectedly, our results show

clearly that steady-state scotopic sensitivity regulation—from the lowest levels that we measure—is mediated primarily by a shortening of scotopic integration time.

Methods

Observers

Three male subjects, AS, LTS TC, served as observers in these experiments. All three had normal color vision according to conventional tests. AS and LTS were highly experienced psychophysical subjects, whereas TC was inexperienced. This study conforms to the standards set by the Declaration of Helsinki, and the procedures were approved by local ethics committees at University College London.

Apparatus

Two or more channels of a five-channel binocular Maxwellian-view optical system were used to project stimuli directly onto the observer's retinas. Three channels originated from a 75-W xenon arc lamp, and two from a 100-W mercury lamp, both run at constant current. Three of the channels had their beams focused in the observer's left pupil; and two in the right pupil. Only two of the five channels were needed for most experiments. The images of the arc in the observer's pupils were less than 2 mm in diameter. Since these images were smaller than the smallest natural pupil, the effective light levels remained unaffected by changes in pupil size. Test and field wavelengths were selected either by the use of 3-cavity, blocked interference filters with full-width at half-maximums (FWHMs) of between 7 and 11 nm (Ealing or Oriel), or by Jobin-Yvon H-10 monochromators with 0.5-mm slits, the spectral outputs of which were triangular functions of wavelength with FWHM bandwidths of c. 4 nm. The radiance of each beam could be controlled by the insertion of fixed neutral-density filters (Oriel) or by the rotation of circular, variable neutral-density filters (Rolyn Optics). Sinusoidal modulation was produced by the pulse-width modulation of fast, liquid crystal light shutters (Displaytech) at a carrier frequency of 400 Hz (components close to which are much too fast to be resolved, so that observers saw only the low-frequency sinusoidal intensity variation produced by the pulse-width modulation). Each shutter had rise and fall times of less than 50 μ s, and could produce sinusoidal modulations with modulation depths ranging from 0 to 92%. Each was driven by computer-controlled programmable timers. The contrast of the shutters measured *in situ* was better than 300:1 at wavelengths longer than 500 nm.

We went to great lengths to eliminate all traces of stray light from the experimental room and apparatus. The most sensitive detector of stray light that was available to us proved to be the fully dark-adapted human eye.

Calibration

The radiant fluxes of the test and adapting fields were measured daily at the plane of the observer’s entrance pupil with a radiometer (Graseby Electronics), which had been cross-calibrated with comparable devices traceable to US and German national standards. Interference filters and monochromators were spectrally calibrated in situ with a spectroradiometer (Gamma Scientific).

Experimental conditions

Target detection was mediated by the rods, except at the highest scotopic luminances, at which cones also contributed to detection (see [Rod isolation](#), below). The transition to cone detection was accompanied by the otherwise gray appearance of the 500-nm target taking on a green tinge. Data that reflect mixed rod and cone detection were not used in the analysis or modeling. We presented the stimuli at eccentricities of 10°. Traditionally, rod experiments are carried out at 15 to 20° in the temporal retina where rod numerosity peaks, but in the binocular experiment we had to avoid the blind spot in the nasal retina of the right eye, and so had to use less eccentric stimuli.

Temporal contrast sensitivity measurements: Temporal contrast sensitivities were measured monocularly at each of the scotopic luminance levels noted in the left column of [Figure 1](#). A 5.7° diameter, 500-nm target was presented at 10° in the temporal retina of the left eye. A small, red centrally viewed cross guided fixation.

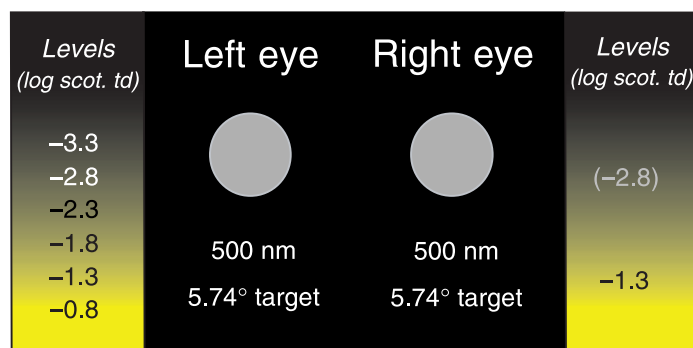


Figure 1. Stimulus configuration and levels of retinal illuminance. Only the left eye stimuli were used for the temporal contrast sensitivity measurements. Both the left and the right eye stimuli were used for the phase delay measurements. The levels are listed in log₁₀ scotopic trolands; that in parentheses was used only for TC.

Phase lag measurements: In these binocular experiments, the target stimulus seen by the left eye was identical to that used to measure temporal contrast sensitivities: a 5.7° diameter, 500-nm green target was presented at 10° in the temporal retina. The target stimulus seen by the right eye was a 5.7° diameter 500-nm green target presented at 10° in the nasal retina. Two small red centrally viewed, crosses in both eyes guided fixation and facilitated binocular fusion.

The levels presented to the left eye were the same as for the modulation or contrast sensitivity measurements (see [Figure 1](#)). The level presented to the right eye was fixed at -1.3 log₁₀ scot. td for AS and LTS, and at -1.3 or -2.8 log₁₀ scot. td for TC. The level measured only in TC is indicated in parentheses. For TC, different standards were used in the right eye for high and low luminance levels, because TC found two flickering lights of very different luminance hard to null perceptually (see below).

Experimental procedures

Subjects dark adapted for 40 minutes before the start of any experiment, and then light adapted to the mean adapting illuminance for 3 minutes before making any settings. Subjects interacted with the computer-controlled Maxwellian-view optical system by means of an 8-button keypad, and received instructions and information from the computer by means of tones and a speech synthesizer.

Temporal contrast sensitivity measurements

Temporal contrast sensitivities were measured by the method of adjustment. Contrast (also known as modulation or ripple ratio), which is defined as:

$$\frac{I_{\max} - I_{\min}}{I_{\max} + I_{\min}}, \tag{1}$$

is given below in terms of rod excitation. An alternative way of visualizing the same threshold is in terms of the flicker amplitude, which we plot as the difference between I_{\max} and I_{\min} . Amplitudes are given below in units of log₁₀ scot. td.

To determine temporal contrast sensitivity, the subject was presented with flickering stimuli and asked to adjust their contrast until the flicker appeared to be just at the threshold. On a single run, three threshold settings were made at each temporal frequency. The data were averaged from four separate runs.

Phase lag measurements

Phase lags were measured using an extension of flicker photometry, in which the subject was instructed to vary

the relative phase as well as the contrast of the two, initially opposite-phase, binocularly fused flickering targets in order to abolish or minimize the appearance of flicker. By pressing keys, the subject could advance or retard the phase in large or small steps, or flip the phase by 180° . If the null covered an extended range of phase delays, which was usually the case if one of the two signals was weak, observers were instructed to set the middle of the phase range.

Three phase settings were made at each temporal frequency in a single experimental run. At least four separate experimental runs were carried out for each condition.

The principle behind using phase adjustments to measure relative perceptual delays is illustrated in Figure 2. When the left and right eyes are adapted to the same luminance level, there should be little delay between the internal signals that they produce. Thus, signals in

opposite phase and equal in amplitude at the input (left, top sequence) should destructively interfere, and produce a flicker null at the output (right, top sequence). When the two eyes are in different states of adaptation so that the signal from the left eye is advanced relative to the right eye signal (by $\Delta\theta = 90^\circ$ in this example), stimuli that are in opposite phase at the input (left, middle sequence) will no longer cancel at the output (right, middle sequence). To restore the null (right, bottom sequence), the subject must delay the left eye stimulus at the input by $\Delta\theta$ (left, sequence). The adjustment required to restore the null provides an estimate of the interocular delay caused by the adaptation difference between the two eyes.

Comparable experiments in which the effects of varying the states of adaptation of the two eyes have been investigated include measurements of Pulfrich's pendulum (e.g., Alpern, 1968; Lit, 1949), and binocular flicker cancellation (e.g., Cavonius & Estévez, 1980; Stockman

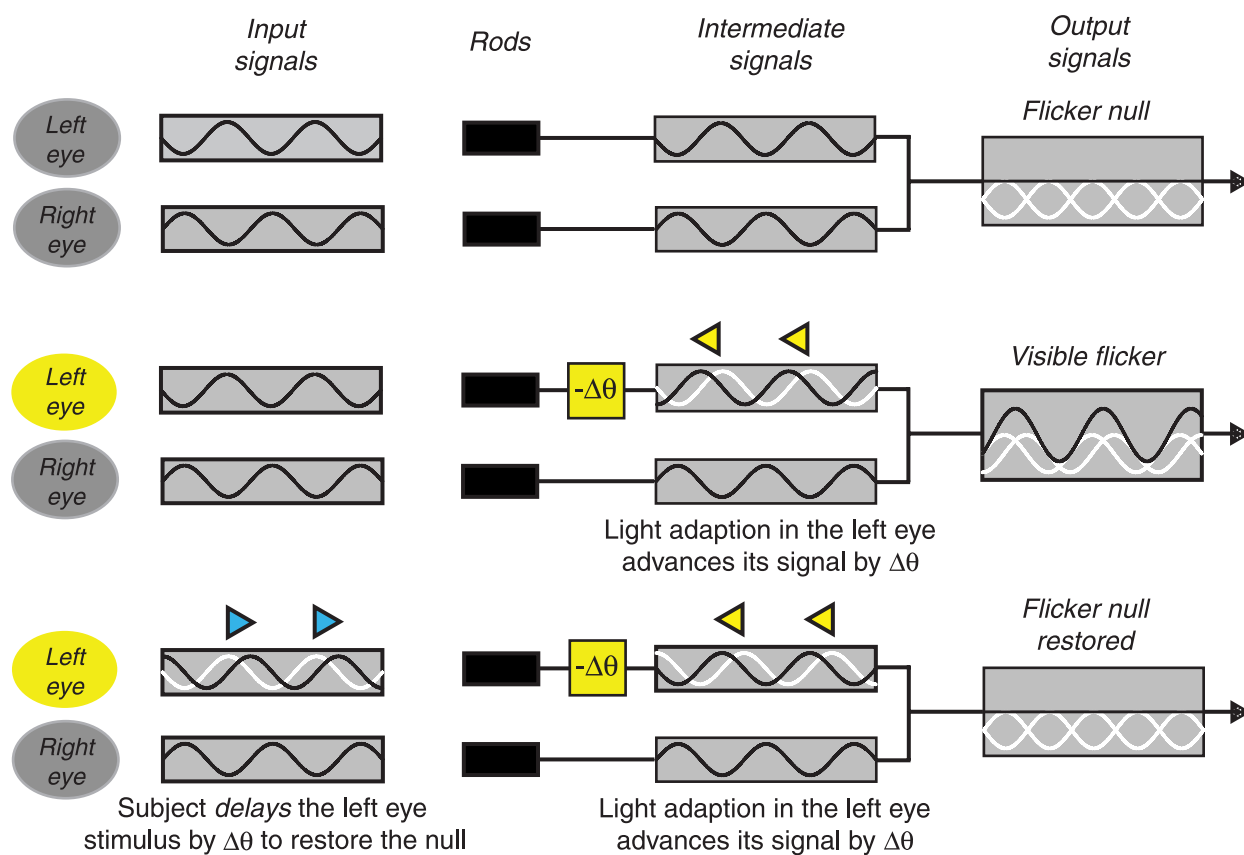


Figure 2. Illustration of the technique used to measure phase delays between stimuli seen by the left and right eyes. Flickering lights are presented separately to the left and right eyes (*Input signals*), which generate neural signals in response to the flicker (*Intermediate signals*). These signals are transmitted to the cortex, where the neural signals from the two eyes are combined (*Output signals*). In the top sequence, the left and right eyes are equally light-adapted, so that there should be little phase delay between the signals from the two eyes. As a result, signals that are in opposite phase at the input (left) should destructively interfere at the output, where they produce a flicker null (right). In the middle and bottom sequences, the left eye is more light-adapted than the right eye, so that the signal in the left eye is phase advanced by $\Delta\theta$ relative to the signal in the right eye. In this case, left and right eye signals in opposition at the input (middle sequence) will no longer null at the output. To restore the null (bottom sequence), the signal seen by the left eye must be phase delayed by $\Delta\theta$ to compensate for the internal phase advance.

et al., 2006), but these were not made under exclusively scotopic conditions.

Rod isolation

Control experiments were carried out to check that the detection sensitivities shown here were determined by rods by making measurements during the cone plateau following a 97% rod bleach. We found that after the bleach, temporal contrast sensitivities could not be measured at any frequency when the mean retinal illuminance was between -3.3 and $-0.8 \log_{10}$ scot. td, which indicates that flicker detection at those levels is mediated primarily by rods. At the next highest level of $-0.3 \log_{10}$ scot td (for which results are not shown), contrast thresholds also could not be measured after the bleach, but the target took on a greenish hue, which indicated some cone involvement. At $0.2 \log_{10}$ scot td, (cone) contrast thresholds could be measured during the cone plateau. Since we were interested only in rod detection with no cone involvement in detection or adaptation, we consider here only the results obtained at levels of $-0.8 \log_{10}$ scot. td and below.

Results

Scotopic temporal contrast sensitivities

Figure 3 shows the scotopic temporal contrast sensitivity functions (TCSFs) for AS (top panel), LTS (middle panel) and TC (bottom panel) measured at six background illuminances ranging from -3.3 to $-0.8 \log_{10}$ scot. td. For all three observers, the shapes of the TCSFs are dependent on the retinal illuminance level. The TCSFs change from steeply falling low-pass functions at the lowest two or three levels to being much broader, slightly bandpass functions at the higher levels. Except between the lowest illuminances, the low-frequency contrast sensitivities remain roughly constant over level, and therefore are consistent with Weber's Law ($\Delta I/I = k$). In contrast, the middle- and high-frequency contrast sensitivities show marked improvements in sensitivity between -3.3 and -1.8 or $-1.3 \log_{10}$ scot. td, and then more modest improvements at still higher illuminances. The highest frequency that can just be detected at 92% contrast (the so-called critical fusion frequency or c.f.f.) increases from about 2 Hz at the lowest levels up to 10 or 12.5 Hz.

There are substantial individual differences between the shapes of the TCSFs for our three observers, which presumably reflect differences in threshold criteria as well as perhaps underlying neural differences. Crucially, however, and despite these differences, the changes in the TCSFs between levels, which reflect the processes of

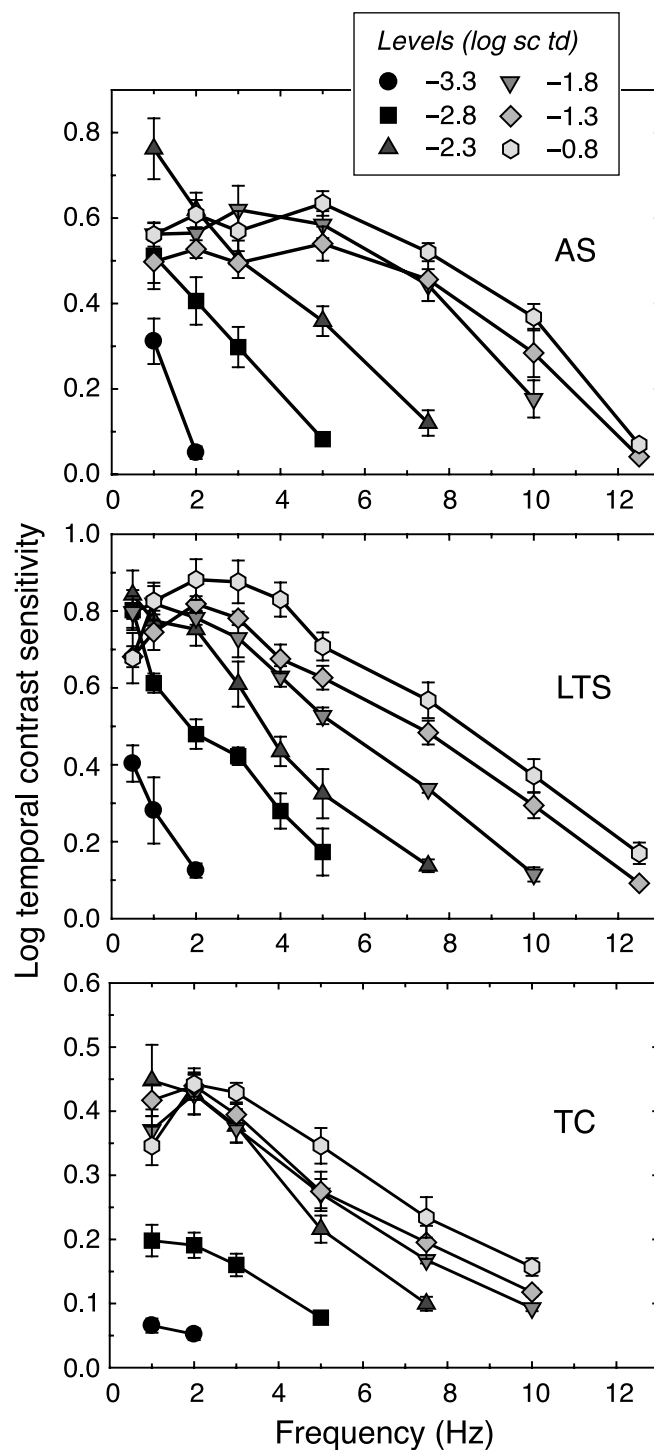


Figure 3. Logarithmic scotopic temporal contrast sensitivities for subjects AS (top panel), LTS (middle panel) and TC (bottom panel) plotted against linear frequency. The adaptation level was varied according to the legend.

light adaptation, are consistent with the operation of the same type of sensitivity regulating mechanism across observers (see below).

Another way of visualizing contrast sensitivity data is to plot them as peak-to-trough threshold amplitudes ($I_{\max} -$

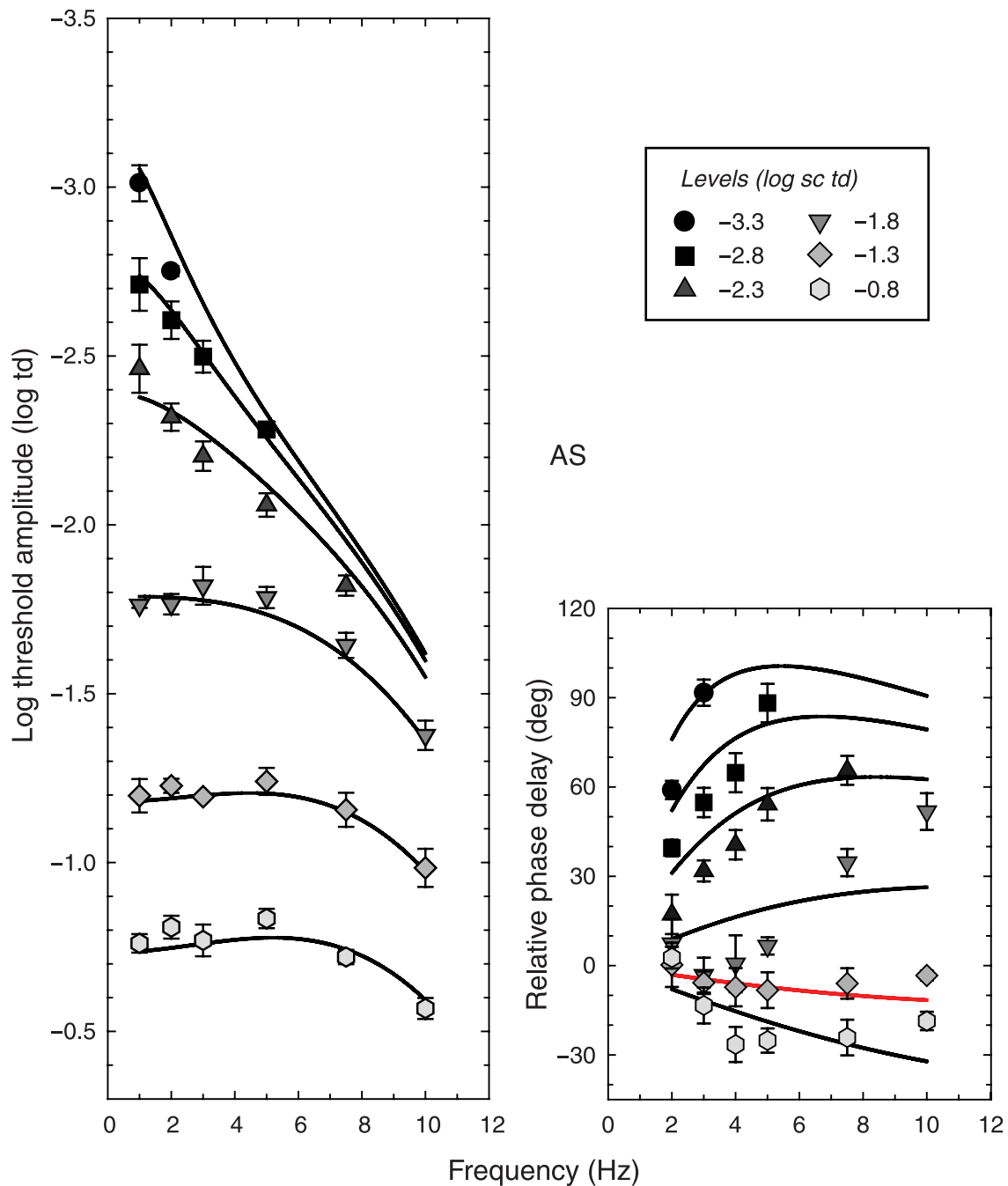


Figure 4. Contrast sensitivities from Figure 3 replotted as logarithmic threshold amplitudes (symbols, left panel) and phase delays (symbols, right panels). The contrast sensitivities were measured in the left eye adapted to the retinal illuminances noted in the legend. The phase delays were measured between the left and right eyes adapted to different retinal illuminances. The illuminance in the right eye was fixed $-1.3 \log_{10}$ scot. td, while that in the left eye was varied according to the legend. The continuous black lines in both panels are reconstructions based on the fits of the shortening integration time model shown in Figure 7, below. The continuous red line in the right panel highlights the phase delays that are assumed to persist even when the two eyes are exposed to the same illuminances. See Discussion for details.

I_{\min}). These are shown in the left panels of Figures 4, 5, and 6 for AS, LTS and TC, respectively. This way of plotting the data not only helps to separate the data points in the figure, but also helps to highlight those levels between which the increase in background illuminance

might not affect threshold amplitude (i.e., when $\Delta I = k$). This constancy, found at high temporal frequencies and known as “high-frequency linearity”, is found in TCSFs measured under photopic conditions (e.g., De Lange, 1958; Kelly, 1972; Roufs, 1972a; Stockman et al.,

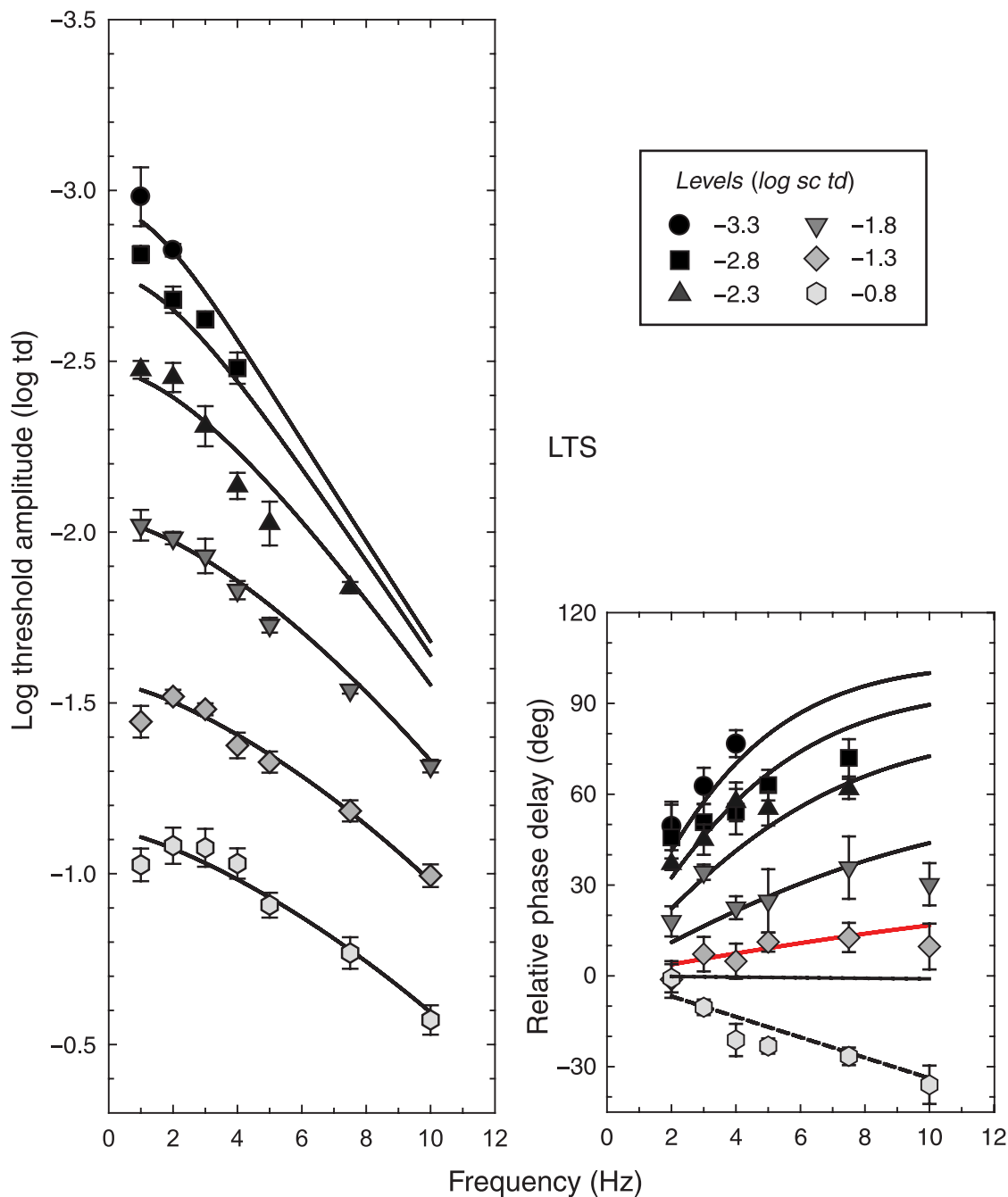


Figure 5. Logarithmic threshold amplitudes, phase delays and model predictions for LTS. The dashed line in the right panel shows the model prediction if an additional delay is allowed between the two highest levels (see Discussion). Other details as Figure 4.

2006). However, it is not found in scotopic TCSFs, as can be seen in these figures. A system that regulates its sensitivity solely by shortening integration times should obey high-frequency linearity, but in the case of the rod system this convergence, if it does indeed occur, does so above the rod c.f.f. and is consequently not measurable.

The continuous lines aligned with both the TCSF and the phase delay data in Figures 4, 5, and 6 are reconstructions based on the model fits shown in Figure 7. They are described in more detail in the Discussion.

Scotopic phase lags

The relative phase delays between rod flicker presented to the left and right eyes are shown in the right panels of Figures 4, 5, and 6, for AS, LTS and TC, respectively. For AS and LTS, the illuminance level in the right eye was fixed throughout at $-1.3 \log_{10}$ scot. td. For TC, the illuminance level in the right eye was fixed either at $-1.3 \log_{10}$ scot td (lower right panel) or at $-2.8 \log_{10}$ scot₁₀ td (upper right panel). As noted above, we used two right

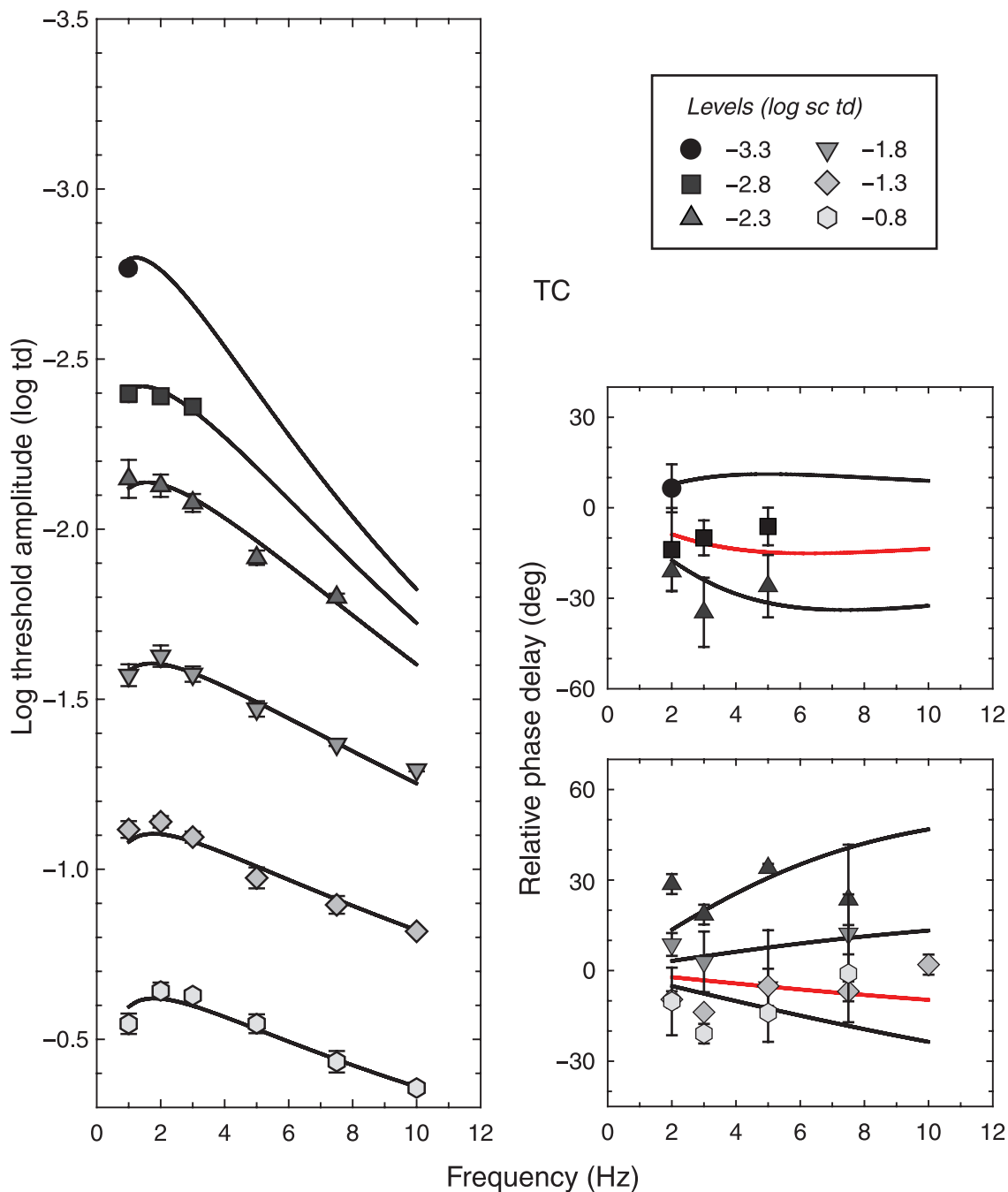


Figure 6. Logarithmic threshold amplitudes, phase delays and model predictions for TC. Details as Figure 4, except that the phase delays are shown in two panels. In the upper panel, the illuminance in the right eye was fixed at $-2.8 \log_{10}$ scot. td, and in the lower panel it was fixed at $-1.3 \log_{10}$ scot. td.

eye levels for TC, because he found it hard to null two flickering lights if their luminances were very different. For each subject, the illuminance in the left eye was varied according to the legend in the figure. A phase delay of zero degrees implies that the phase delays introduced by the left and right eye visual pathways are the same. A positive delay indicates that the flicker shown to the left eye had to be advanced away from opposite phase to optimize the

null-presumably to compensate for a relative delay in the signal generated by that eye. By contrast, a negative delay indicates that the flicker in the left eye had to be delayed to optimize the null-presumably to compensate for a relative advance in the signal generated by that eye. The phase delays for all three subjects show similar trends.

The phase delays measured at the same retinal illuminance in the two eyes (gray diamonds, and, for TC, also

filled squares) are, as expected, roughly 0° . Decreasing the adaptation level in the left eye requires an advance in the flicker to compensate for an increase in phase delay, because that eye is less light adapted. Increasing the adaptation level in the left eye requires a delay in the flicker to compensate for a decrease in phase delay, because that eye is more light adapted.

When the two eyes are exposed to the same background level (i.e., $-1.3 \log \text{scot}_{10} \text{ td}$ for AS and LTS, and -2.8 or $-1.3 \log \text{scot}_{10} \text{ td}$ for TC), the phase settings for all three subjects are offset from 0° . Those for AS and TC are slightly phase advanced, which suggests that the left eye is effectively slightly more light adapted than the right eye (despite being exposed to the same illuminance level), while those for LTS are slightly phase delayed, which suggests that right eye is slightly more light adapted. Given that these offsets were reproducible over the several months of the experiment, we believe that they are real and not due to some experimental artifact such as a calibration error or misalignment. The differences presumably also reflect the fact that the stimuli in the two eyes were presented to retinal areas that are different distances from the optic nerve. However, the 20° difference in the positions of the two targets is likely to cause an additional delay of less than one millisecond (less than 3.6° at 10 Hz), given the typical transmission speeds of ganglion cell axons (e.g., Kaplan & Shapley, 1982; Schiller & Malpeli, 1977). Whatever their cause, these offsets do not affect the model fits shown in Figures 7 and 8 below. They do, however, affect the reconstructions of the phase delays shown in Figures 4, 5, and 6 and described in the next section.

Comparisons between the left and right panels of Figures 4, 5, and 6 show that large frequency-dependent changes in the shapes of the amplitude sensitivity functions between levels are invariably accompanied by large frequency-dependent changes in phase delay. These correlated changes are strongly suggestive of a shortening of the scotopic integration time with adaptation.

Discussion

The correlated frequency-dependent changes in sensitivity and phase found for all three observers evident in Figures 4, 5, and 6 demonstrate convincingly that steady-state sensitivity regulation is accompanied over most of the scotopic range by a speeding up or slowing down the scotopic response. The data show clearly that phase advances are correlated with relative improvements in high-frequency temporal contrast sensitivity, and (equivalently) phase delays are correlated with relative losses in high-frequency sensitivity. Moreover, because the rates of photon absorptions per rod are too low to sustain effective receptor sensitivity regulation over much of the scotopic

range (see above), these speed changes must be implemented largely after the photoreceptors.

Relation to other psychophysical data

Our TCSF data are consistent with the TCSF data of Nygaard and Frumkes (1985), who also found relative sensitivity improvements at higher temporal frequencies, and with the results of the elegant two-target experiments of van den Brink and Bouman (1954), who measured the thresholds for detecting pairs of subthreshold targets at a series of retinal illuminances as a function of the delay between them. Temporal integration time can be estimated from the two-target data on the assumption that the threshold is lower when both targets fall within the integration time. Figure 2 of van den Brink and Bouman (1954) provides clear evidence for changes in temporal integration time in the scotopic range.

Our TCSF data, however, are seemingly inconsistent with other TCSF data in which evidence for only frequency-independent sensitivity-scaling was found. One reason for the inconsistencies is that in some studies the luminances were restricted to relatively high scotopic levels, and so missed the more pronounced changes in the shapes of the TCSFs, which, as can be seen in Figure 3, occur below $-1.8 \log_{10} \text{scot. td}$. Two studies fall into this category: Smith (1973), who made measurements only above $-1.70 \log_{10} \text{scot. td}$ and Sharpe et al. (1989), who made them only above $-1.32 \log_{10} \text{scot. td}$. However, even in those studies in which TCSFs were measured below $-1.8 \log_{10} \text{scot. td}$, our modeling (see Figures 7 and 8, below) suggests that it would be hard to exclude scaling as the primary sensitivity regulating mechanism without the much more diagnostic phase-delay data.

Our measured phase delays contradict the monocular rod-cone phase measurements of Sharpe et al. (1989), who found little or no change in rod phase delay between -1.6 and $-0.3 \log_{10} \text{scot. td}$ when measured against a cone standard. By contrast, in the overlapping range of -1.8 to $-0.8 \log_{10} \text{scot. td}$ used here, we find substantial reductions in phase delay for observers AS and LTS (the same observers, in fact, used in the earlier studies). We suspect that these discrepancies are due to the modest levels of cone excitation required in the Sharpe et al. (1989) study to produce the cone standard, which may have indirectly altered the state of scotopic adaptation. By using a binocular rod standard, we were able to avoid significant cone excitation in this study.

For reasons outlined in the Introduction, our results are also inconsistent with the lack of any slope differences found between the logarithmic slopes of rod TVI functions measured using 10 and 200-ms flashes (Sharpe et al., 1993). The temporally broad-band nature of 10- and 200-ms flashes makes these TVI measurements difficult to model with any certainty, but based on our results and model we would have expected some slope differences.

A problem with scotopic studies, in general, and one that we have hopefully avoided here, is that the presence of any stray light would artifactually limit the lowest scotopic illuminances that could actually be produced, and therefore limit the extent of the adaptation-dependent changes found.

Light adaptation models

In this section, we use our data to evaluate different models of scotopic sensitivity regulation and thus identify the classes of mechanism that regulate sensitivity. We distinguish between three broad, not necessarily mutually exclusive, classes of sensitivity regulating mechanisms:

1. *Mechanisms that alter the scotopic integration time.* Such mechanisms are assumed to cause changes in the shapes of the TCSFs and corresponding changes in phase delay. One caveat is that if the integration time is already short, shortening it further will not change the shape of the TCSF in the range of visible temporal frequencies (see Equation 2).
2. *Mechanisms that alter sensitivity solely by scaling or response compression.* Such mechanisms are assumed to shift the logarithmic TCSFs vertically without changing their shape, but are assumed to leave the phase delays unaffected.
3. *Mechanisms that alter the visual delay.* Such mechanisms are assumed to cause characteristic changes in phase that are linear with frequency (see Equation 4), but are assumed to leave the TCSFs completely unaffected.

In generating the following models, we readily acknowledge our debt to previous modelers, many of whom used the same elements we used (e.g., Baylor & Hodgkin, 1974; Baylor, Hodgkin, & Lamb, 1974; De Lange, 1958, 1961; Kelly, 1961; Matin, 1968; Penn & Hagins, 1972; Roufs, 1972b; Sperling & Sondhi, 1968; Tranchina, Gordon, & Shapley, 1984; Watson, 1986).

It is important to note that because the phase delay measures are necessarily relative ones, we do not know the absolute phase delays associated with the scotopic system. Consequently, we have limited our models of scotopic sensitivity regulation to account only for the *relative* changes in phase delay and the *relative* changes in contrast sensitivity that occur between the successive levels shown in Figures 4, 5, and 6. These differences are plotted as symbols in Figures 7 and 8.

Shortening integration time

We start by modeling our data solely in terms of shortening the integration time. We take the now classic

approach of implementing the changes in integration time by shortening or lengthening the time constants (τ) of one or more (n) cascaded leaky integrating stages (or buffered RC circuits or low-pass filters). The formula for the amplitude response, $A(f)$, of n cascaded leaky integrators is:

$$A(f) = \tau^n \left[(2\pi f \tau)^2 + 1 \right]^{-\frac{n}{2}}, \quad (2)$$

and the phase response, $P(f)$, is:

$$P(f) = n \tan^{-1}(2\pi f \tau), \quad (3)$$

where f is frequency in cycles per second (Hz), and τ is the time constant in seconds. For further information, see, for example, Watson (1986). This approach is still relevant in the modern context of molecular processes in the sense that leaky integrators can be associated with first-order biochemical reactions.

The left panels of Figure 7 show the changes in contrast sensitivity plotted as changes in amplitude, and the right panels show the changes in phase delay. Data for AS, LTS and TC are shown in the top, middle and bottom panels, respectively.

In optimizing the model parameters, the time constants of the n filters were varied together, thus altering the threshold amplitudes according to Equation 2 and the phase delays according to Equation 3. Allowing the time constants of each filter to vary independently yielded additional parameters, but did not significantly improve the predictions. The phase and amplitude data were weighted so that their influence was approximately equal (otherwise one or other set of data would dominate the fitting procedure). The number of filters, n , was allowed to take on non-integer values in preliminary fits. A value of $n = 2$ was used for the final fits, because this represented the best estimate across all three subjects. We emphasize, however, that n is poorly constrained by the fit, because increases in n can be offset by decreases in τ and vice versa. Thus, $n = 2$ should be considered approximate, because values of $n > 2$ would also produce plausible fits. In contrast, a value of $n = 1$ is implausible, because it would limit the maximum phase change to 90° , which is less than the measured changes (see Figures 4, 5, and 6). The model fits for $n = 2$ are shown by the continuous lines in Figure 7 coded using the same colors as the symbols.

Given that with n fixed at 2 there is only a single intensity-dependent parameter, τ , the fits to the phase and amplitude data shown in Figure 7 are fairly good. (The change in τ with retinal illuminance for each subject is shown in the lower panel of Figure 9, below.) Relative to the null model that there is no change in amplitude or phase between levels (i.e., all the values in Figure 7 are zero and therefore there is effectively no adaptation), the

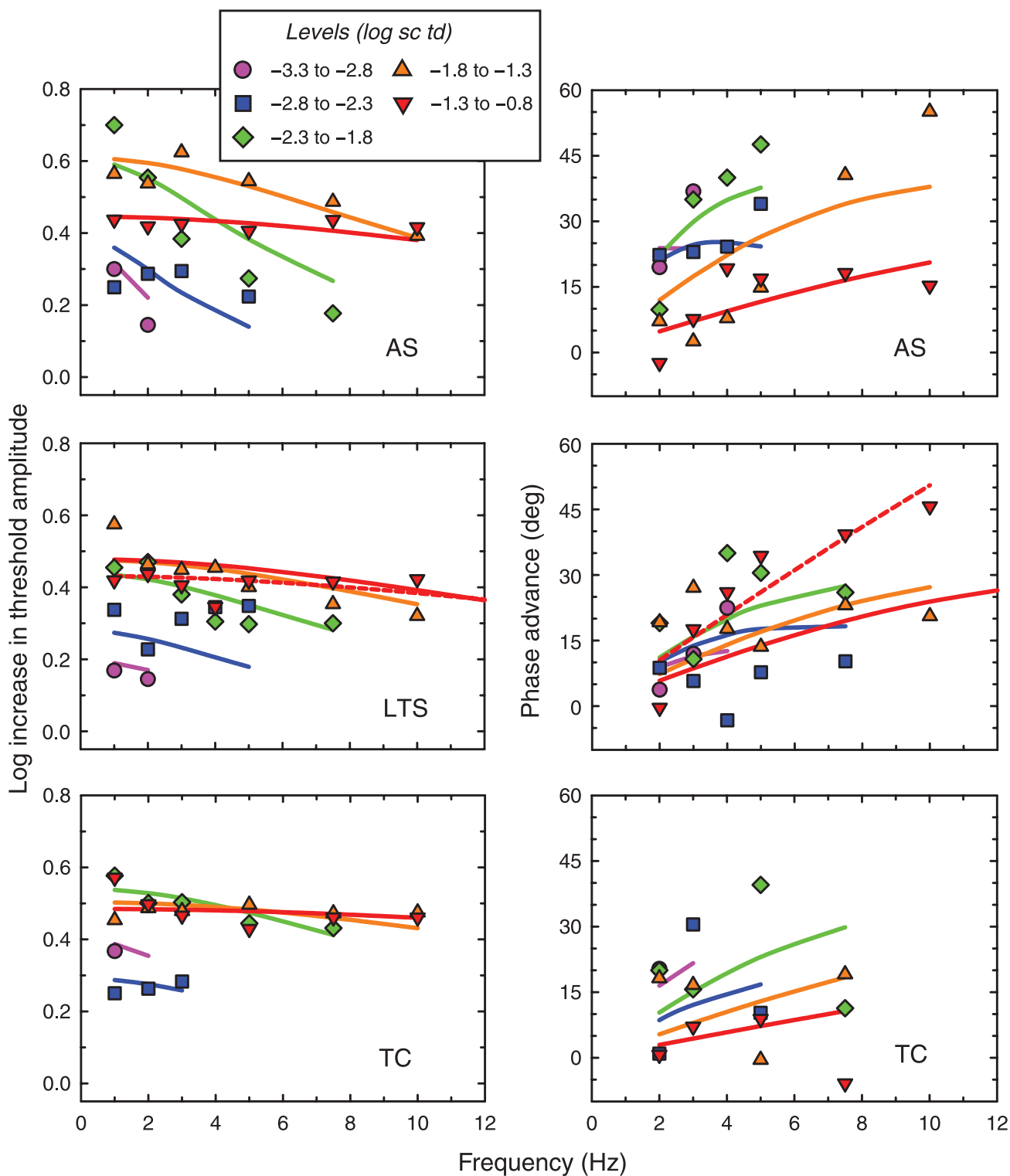


Figure 7. Simultaneous fits of the integration time model (continuous lines) to the amplitude differences (symbols, left panels) and phase delay differences (symbols, right panels) between successive levels for AS (top panels), LTS (middle panels) and TC (lower panels). The dashed line shown in the right panel for LTS shows the fit between the two highest levels with an additional time advance of 9.06 ms.

single-parameter model accounts for 97.97% of the threshold amplitude and 89.20% of the phase variance for AS, 96.37% of the threshold amplitude and 75.33% of the phase variance for LTS; and 99.52% of the threshold

amplitude and 61.99% of the phase variance for TC. The amplitude fits are generally good, but the phase fits are poorer. Nonetheless, the single parameter model accounts for most of the variance. For TC, the deviations of the

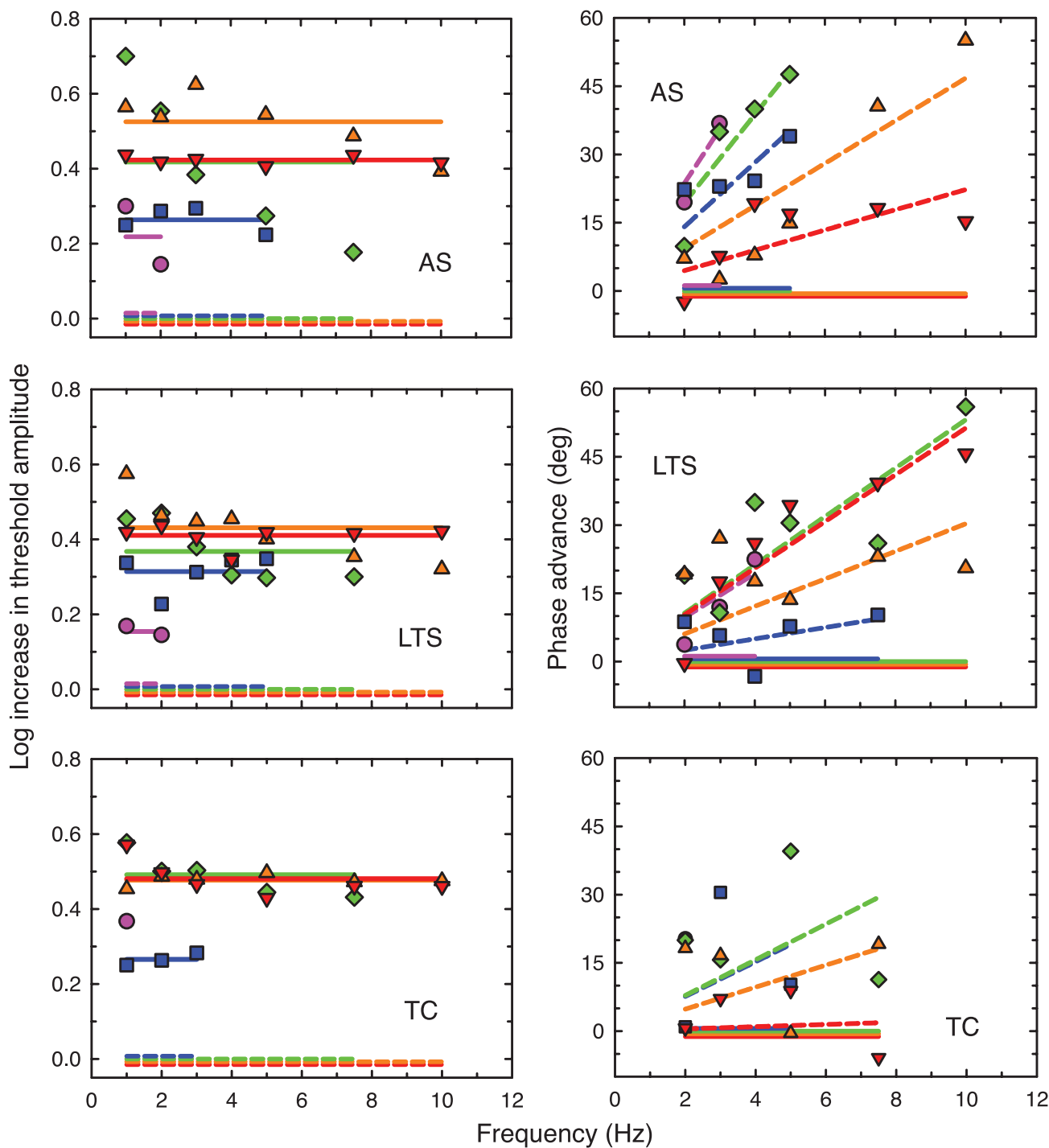


Figure 8. Simultaneous fits of either the sensitivity scaling model (continuous lines) or the time delay model (dashed lines) to the amplitude differences (symbols, left panels) and phase delay differences (symbols, right panels) between levels. Note that, as indicated, the sensitivity scaling model predicts no changes in time delay between successive levels, and the sensitivity scaling model predicts no changes in phase. Other details as [Figure 7](#).

phase delays from the model predictions have no obvious structure, and reflect in part the difficulties he had in setting binocular phase delays. For LTS, there is a clear discrepancy in the phase predictions between the two highest levels, where the model seriously underestimates the phase advance. We speculate that this discrepancy is

associated with the intrusion of the faster rod pathway (e.g., Sharpe & Stockman, 1999), which seems to become prominent at a lower level for LTS than for the other subjects. We account for this faster pathway by adding an additional time advance of 9.06 ms between the two highest levels; the model then accounts for 98.78% of the

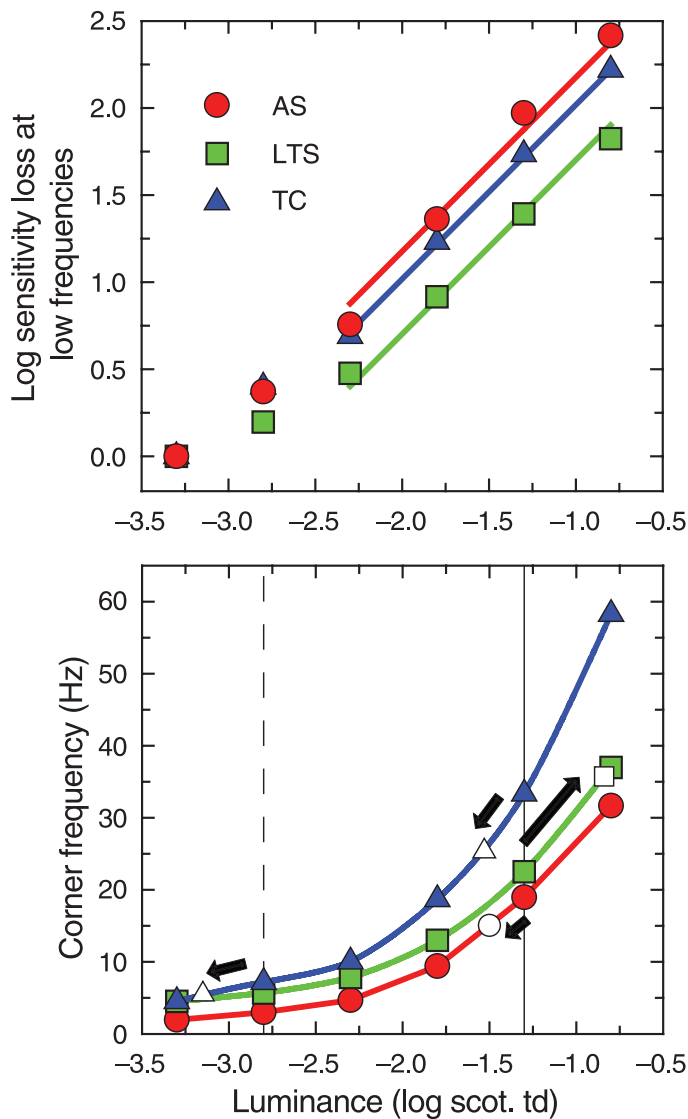


Figure 9. Properties of the 2-stage integration-time model for AS (red circles), LTS (green squares) and TC (blue triangles). The colored symbols in the lower panel show the time constants, τ , of the two lowpass filters plotted as the corner or cut-off frequencies of the filters, $1/(2\pi\tau)$. These correspond to the model fits shown in Figure 7 and reflect the state of adaptation assumed in the left eye. The vertical lines correspond to the background luminances presented to the right (reference) eye during the phase delay measurements for AS, LTS and TC (solid line) and for TC (dashed line). The open symbols are estimates of the corner frequencies of the two lowpass filters in the right eye when the left and right eyes are exposed to the same luminance levels. The open symbols have been shifted along the abscissa to align with the scotopic luminances in the left eye that produce the same corner frequencies in that eye. The differences between the two eyes are indicated by the arrows, which point from the corner frequency assumed in the left eye to that assumed in the right eye. The symbols in the upper panel show the logarithmic sensitivity losses at *low* temporal frequencies caused by the shortening time constants. The straight lines fitted to the symbols have a slope of one consistent with Weber's Law.

amplitude and 91.86% of the phase variance. This speculative modification to the model predictions is shown by the dashed lines for LTS in Figure 7.

Sensitivity scaling

As a comparison, we next modeled our data solely in terms of sensitivity scaling; that is, we assumed that the differences between the TCSFs can be accounted for by multiplying the sensitivities by a constant scaling factor. On the logarithmic scale of Figure 8 this equates to adding or subtracting a constant. The fits are shown by the solid lines in the figure. (Because no changes in phase are predicted, the fits shown in the right panels as solid lines are all at zero.) The fits to the amplitude data shown in the left panels are reasonably good. Relative to their being no adaptational changes, the model accounts for 94.65%, 97.82 and 99.34% of the threshold amplitude variance for AS, LTS and TC, respectively, but, of course, 0% of the phase delay variance. In terms of the variance accounted for, the sensitivity scaling model does as well as the shortening integration time model in accounting for the changes in contrast sensitivity. Consequently, in the absence of the phase delay data, we would not be able to distinguish between the two models, and we might well have concluded—like earlier workers—that scotopic sensitivity regulation was achieved primarily by scaling or response compression.

Changing time delay

As a further comparison, we modeled our data solely in terms of changes in time delay; that is, we assumed that the differences between the phase delays can be accounted for by adding or subtracting a time difference. The change in phase delay, $\Delta P(f)$, in degrees is related to a time difference of Δt in seconds by:

$$\Delta P(f) = 360\Delta t f, \quad (4)$$

where f is frequency in Hz. In the model we allowed Δt to vary between levels. The fits of the model are shown in Figure 8 as the dashed lines. (Because no changes in amplitude are predicted, the fits shown in the left panels as dashed lines are all at zero.) The fits to the phase delay data shown in the right panels are fairly good for AS and LTS. Relative to there being no adaptational changes, the model accounts for 94.35%, 87.78 and 60.09% of the phase variance for AS, LTS and TC, respectively, but 0% of the amplitude variance. In fact, the time delay model actually does a slightly better job of accounting for the phase data than shortening the integration time. In the absence of the amplitude data, we might reasonably conclude that the rod system speeds up its response as the light level increases by decreasing its response delay.

Mixed models

Rather than develop arbitrarily complex models to better account for the data, we have chosen to restrict our development to the combination of the three classes of sensitivity regulating mechanisms previously described. That is, we combined shortening integration times either with (i) sensitivity scaling or (ii) changing time delays. The model fits are not shown graphically. Relative to the null model, the shortening integration time plus sensitivity scaling model accounts for 98.42% of the threshold amplitude and 92.24% of the phase variance for AS; 98.04% of the threshold amplitude and 91.16% of the phase variance for LTS; and 99.25% of the threshold amplitude and 72.12% of the phase variance for TC. Comparable improvements are found with the shortening integration time plus time delay model, which accounts for 97.79% of the threshold amplitude and 92.52% of the phase variance for AS; 98.31% of the threshold amplitude and 89.06% of the phase variance for LTS; and 99.29% of the threshold amplitude and 70.23% of the phase variance for TC.

Not surprisingly, the addition of an extra intensity-dependent fitting parameter improves the fits. The reductions in amplitude variance, however, are small. The main improvements are reductions in phase variance of about 3% for AS, 4 or 5% for LTS and 8 or 10% for TC. Given these fairly modest improvements, and the fact that the changes in either scaling or time delay implied by these models (not shown) are inconsistent across subjects, we have retained the simple integration time model as our qualitative description of scotopic sensitivity regulation.

In our earlier work on cone adaptation (Stockman et al., 2007, 2006), we also found that an integration time model could account for most of the amplitude and phase variance below bleaching levels, but in our final qualitative model we also incorporated sensitivity scaling. This was necessary to account for bleaching at high levels, and also to account for an unexpected sensitivity improvement suggested at lower adaptation levels, which we related to increasing the sensitivity of gated ion channels and increasing rates of molecular resynthesis (Stockman et al., 2006). These processes may be absent in postreceptoral scotopic sensitivity regulation, but our data cannot exclude them.

Reconstructing the original data from the model predictions

The 2-stage integration-time model, and the other models described above, predict only the relative changes in sensitivity and phase with adaptation. They do not predict the original data shown in Figures 4, 5, and 6, but we can map the model predictions onto the original data by making a few simple additional assumptions (which have no direct bearing on the models).

The reconstruction of the absolute amplitude data shown in the left panels of Figures 4, 5, and 6 from the

relative changes in amplitude predicted by the model (and shown in Figure 7) requires that we assume an arbitrary constant at each frequency, which is independent of the adaptation level, and which allows us to reconstruct the absolute amplitude values from the relative ones. Largely for aesthetic reasons, we have assumed that these arbitrary constants should form a single smooth curve (or template) as a function of frequency. For each observer, therefore, we derived a smooth template shape that, when combined with the relative model predictions, best fit the amplitude threshold data.

We achieved this by applying the 2-stage integration model and model parameters to adjust all the amplitude data to the common level of $-1.80 \log_{10}$ scot. td. We then used a curve discovery program (TableCurve 2D, Jandel) to find a best-fitting smooth template to account for all the adjusted data. This template was then used to reconstruct the amplitude thresholds from the relative amplitude predictions. The smooth templates for each subject can be seen as the functions fitted to the amplitude data at $-1.80 \log_{10}$ scot. td in the left panels of Figures 4, 5, and 6. We attach no special significance to these functions, the formulae for which are not given.

The reconstruction of the phase data shown in the right panels of Figures 4, 5, and 6 from the relative changes in phase predicted by the 2-stage integration-time model is complicated by the non-zero phase delays that persist even when the two eyes are exposed to the same background luminances (see above).

We have incorporated these non-zero phase delays by allowing a small adaptation-independent difference in time constant between the two eyes. We define this difference relative to the time constant assumed to apply in the left eye when exposed to the same background as the right eye (the time constants assumed in the left eye are plotted as corner frequencies in Figure 9). [The corner frequency is related to the time constant, τ , by $1/(2\pi\tau)$]. Using the 2-stage integration-time model, we determined the difference in time constant between the right and left eyes that produced the best-fit for each subject between the model predictions shown in Figure 7 and the phase measurements shown in Figures 4, 5, and 6. In terms of corner frequencies, the changes from left to right eye at $-1.30 \log_{10}$ scot. td were 18.95 to 15.05 Hz for AS, 22.50 to 35.75 Hz for LTS, and 33.34 to 25.33 Hz for TC, and at $-2.80 \log_{10}$ scot. td 7.17 to 5.50 Hz for TC. These changes are highlighted by the arrows in the lower panel of Figure 9, each of which points from the corner frequency assumed in the left eye (colored symbol) to the best-fitting value found in the right eye (open symbol). (The open symbols have been aligned with the scotopic luminances in the left eye that produce the same corner frequencies.) The changes in corner frequency for AS and TC are modest, but those for LTS are surprisingly large.

The phase delays generated by the changes in corner frequency are shown in the right panels of Figures 4, 5, and 6 as the continuous red lines. These functions account

plausibly well for the phase delays when the two eyes are adapted to the same luminance levels. Having thus defined the fixed phase delays between the two eyes, it is straightforward to reconstruct the measured phase delays from the relative predictions shown in Figure 7. These are shown by the continuous black lines in the right panels of Figures 4, 5, and 6. The reconstruction shown as the dashed line for LTS includes the additional assumption of a time advance of 9.06 ms between the two highest levels (see above).

Although there are some discrepancies, the adjusted templates describe the data remarkably well over the entire range of illuminance levels.

We emphasize again that the assumptions made in reconstructing the original data from the model predictions have no direct bearing on the underlying model.

Properties of the 2-stage integration time model

The time constants, τ , of the two lowpass filters that make up the integration time model are plotted as the corner or cut-off frequencies of the filters, $1/(2\pi\tau)$, in the lower panel of Figure 9 for AS (red circles), LTS (green squares) and TC (blue triangles). These cut-off frequencies, which indicate the frequency after which the attenuation of the filter sharply increases, can be usefully compared with the TCSF data. For all three subjects, the cut-off frequencies increase steadily over the entire scotopic range. At higher retinal illuminances, these adaptively modifiable filters selectively attenuate relatively little over the range of frequencies that can be seen with scotopic vision. Note the model only incorporates modifiable filters. There will be, in addition, filters the temporal characteristics of which do not change with light level.

The symbols in the upper panel show the logarithmic sensitivity losses at low frequencies caused by the shortening time constants. The straight lines fitted to the symbols have a slope of one, which is consistent with Weber's Law. Thus, the decrease in the time constants of the two filters in the model is tuned to give Weber's Law for low temporal frequencies. In other words, $\tau = kI^{-1/n}$, so that for $f = 0$ Equation 2 becomes: $A(0) = k^n I^{-1}$, where k is a constant of proportionality. In our version of the model, $n = 2$, but as noted above this could take on other values and still account well for the data.

Conclusions

Despite the sizeable individual differences in the TCSFs and phase delays, the changes in the scotopic temporal response with adaptation for all three subjects can be accounted for by shortening the time constants of a cascade of approximately two leaky integrators. Thus, the scotopic system's ability to detect a few photons yet still be able to

operate at higher scotopic levels is achieved mainly by shortening the scotopic integration time. Apparently, the scotopic visual system is exquisitely designed to trade unneeded sensitivity (roughly in accordance with Weber's Law at low temporal frequencies) for improvements in temporal resolution and response speed. Given the low photon count per rod over much of the scotopic range, the changes in temporal integration must occur largely post-receptorally.

Acknowledgments

This work was supported by the BBSRC and Fight for Sight. We thank Bruce Henning for comments and for helpful discussions. Thanks also to John Robson for the original suggestion made many years ago to make binocular measurements of phase delay.

Commercial relationships: none.

Corresponding author: Andrew Stockman.

Email: a.stockman@ucl.ac.uk.

Address: Department of Visual Neuroscience, Institute of Ophthalmology, 11-43 Bath Street, London, EC1V 9EL, UK.

References

- Aguilar, M., & Stiles, W. S. (1954). Saturation of the rod mechanism of the retina at high levels of stimulation. *Optica Acta*, *1*, 59–64.
- Alpern, M. (1968). A note on visual latency. *Psychological Review*, *75*, 260–264. [PubMed]
- Arshavsky, V. Y., Lamb, T. D., & Pugh, E. N., Jr. (2002). G proteins and phototransduction. *Annual Review of Physiology*, *64*, 153–187. [PubMed]
- Barlow, H. B. (1957). Increment threshold at low intensities considered as signal/noise discriminations. *The Journal of Physiology*, *136*, 469–488. [PubMed]
- Barlow, H. B., & Levick, W. R. (1969). Three factors limiting the reliable detection of light by retinal ganglion cells of the cat. *The Journal of Physiology*, *200*, 1–24. [PubMed]
- Baumgardt, E. (1949). Les théories photochimiques classiques et quantiques de la vision et l'inhibition nerveuse en vision liminaire. *Revue d'optique théorique et instrumentale*, *28*, 453–661, 661–669.
- Baylor, D. A., & Hodgkin, A. L. (1974). Changes in time scale and sensitivity in turtle photoreceptors. *The Journal of Physiology*, *242*, 729–758. [PubMed] [Article]
- Baylor, D. A., Hodgkin, A. L., & Lamb, T. D. (1974). The electrical response of turtle cones to flashes and steps

- of light. *The Journal of Physiology*, 242, 685–727. [[PubMed](#)] [[Article](#)]
- Baylor, D. A., Nunn, B. J., & Schnapf, J. L. (1984). The photocurrent, noise and spectral sensitivity of rods of the monkey *Macaca fascicularis*. *The Journal of Physiology*, 357, 575–607. [[PubMed](#)] [[Article](#)]
- Burns, M. E., & Baylor, D. A. (2001). Activation, deactivation and adaptation in vertebrate photoreceptor cells. *Annual Review of Neuroscience*, 24, 779–805. [[PubMed](#)]
- Cavonius, C. R., & Estévez, O. (1980). Applications of signal-processing methods in visual psychophysics. In M. Kunt & F. de Coulon (Eds.), *Signal processing: Theories and applications* (pp. 343–349). Amsterdam: North-Holland Publishing Company.
- Cicerone, C. M., & Hayhoe, M. M. (1990). The size of the pool for bleaching adaptation in human rod vision. *Vision Research*, 30, 693–697. [[PubMed](#)]
- Conner, J. D. (1982). The temporal properties of rod vision. *The Journal of Physiology*, 332, 139–155. [[PubMed](#)] [[Article](#)]
- Conner, J. D., & MacLeod, D. I. A. (1977). Rod photoreceptors detect rapid flicker. *Science*, 195, 689–699. [[PubMed](#)]
- De Lange, H. (1958). Research into the dynamic nature of the human fovea-cortex systems with intermittent and modulated light: I. Attenuation characteristics with white and colored light. *Journal of the Optical Society of America*, 48, 777–784.
- De Lange, H. (1961). Eye's response at flicker fusion to square-wave modulation of a test field surrounded by a large steady field of equal mean luminance. *Journal of the Optical Society of America*, 51, 415–421.
- Dowling, J. E. (1967). The site of visual adaptation. *Science*, 155, 273–279. [[PubMed](#)]
- Dunn, F. A., Doan, T., Sampath, A. P., & Rieke, F. (2006). Controlling the gain of rod-mediated signals in the mammalian retina. *Journal of Neuroscience*, 26, 3959–3970. [[PubMed](#)] [[Article](#)]
- Dunn, F. A., & Rieke, F. (2008). Single-photon absorptions evoke synaptic depression in the retina to extend the operational range of rod vision. *Neuron*, 57, 894–904. [[PubMed](#)] [[Article](#)]
- Enroth-Cugell, C., & Shapley, R. M. (1973). Adaptation and dynamics of cat retinal ganglion cells. *The Journal of Physiology*, 233, 271–309. [[PubMed](#)] [[Article](#)]
- Frishman, L. J., & Sieving, P. A. (1988). Evidence for two sites of adaptation affecting the dark-adapted ERG of cats and primates. *Vision Research*, 35, 435–442. [[PubMed](#)]
- Graham, N., & Hood, D. C. (1992). Modeling the dynamics of adaptation: The merging of two traditions. *Vision Research*, 32, 1373–1393. [[PubMed](#)]
- Hamer, R. D., Nicholas, S. C., Tranchina, D., Lamb, T. D., & Jarvinen, J. L. P. (2005). Toward a unified model of vertebrate rod phototransduction. *Visual Neuroscience*, 22, 417–436. [[PubMed](#)] [[Article](#)]
- He, S., & MacLeod, D. I. A. (2000). Spatial and temporal properties of light adaptation in the rod system. *Vision Research*, 40, 3073–3081. [[PubMed](#)]
- Hess, R. F., & Nordby, K. (1986). Spatial and temporal limits of vision in the achromat. *The Journal of Physiology*, 371, 365–385. [[PubMed](#)] [[Article](#)]
- Hood, D. C. (1998). Lower-level visual processing and models of light adaptation. *Annual Review of Psychology*, 49, 503–535. [[PubMed](#)]
- Hood, D. C., & Birch, D. G. (1993). Light adaptation of the human rod receptors: The leading edge of the human a-wave and models of rod receptor activity. *Vision Research*, 33, 1605–1618. [[PubMed](#)]
- Hood, D. C., & Finkelstein, M. A. (1986). Sensitivity to light. In K. Boff, L. Kaufman, & J. Thomas (Eds.), *Handbook of perception and human performance* (vol. 1, pp. 5-1–5-66). New York: Wiley.
- Kaplan, E., & Shapley, R. M. (1982). X and Y cells in the lateral geniculate nucleus of the macaque monkeys. *The Journal of Physiology*, 330, 125–143. [[PubMed](#)] [[Article](#)]
- Kelly, D. H. (1961). Visual responses to time-dependent stimuli: I. Amplitude sensitivity measurements. *Journal of the Optical Society of America*, 51, 422–429. [[PubMed](#)]
- Kelly, D. H. (1972). Flicker. In D. Jameson & L. H. Hurvich (Eds.), *Handbook of sensory physiology* (vol. VII/4, pp. 273–302). Berlin: Springer-Verlag.
- Kraft, T. W., Schneeweis, D. M., & Schnapf, J. L. (1993). Visual transduction in human rod photoreceptors. *The Journal of Physiology*, 464, 747–765. [[PubMed](#)] [[Article](#)]
- Lennie, P. (1979). Scotopic increment thresholds in retinal ganglion cells. *Vision Research*, 19, 425–430. [[PubMed](#)]
- Lit, A. (1949). The magnitude of the Pulfrich stereophenomenon as a function of binocular differences of intensity at various levels of illumination. *American Journal of Psychology*, 62, 159–161. [[PubMed](#)]
- MacLeod, D. I. A. (1978). Visual sensitivity. *Annual Review of Psychology*, 29, 613–645. [[PubMed](#)]
- MacLeod, D. I. A., Chen, B., & Crognale, M. (1989). Spatial organization of sensitivity regulation in rod vision. *Vision Research*, 29, 965–978. [[PubMed](#)]
- MacLeod, D. I. A., & He, S. (1993). Visible flicker from invisible patterns. *Nature*, 361, 256–258. [[PubMed](#)]
- MacLeod, D. I. A., Williams, D. R., & Makous, W. (1992). A visual nonlinearity fed by single cones. *Vision Research*, 32, 347–363. [[PubMed](#)]
- Matin, L. (1968). Critical duration, the differential luminance threshold, critical flicker frequency, and visual

- adaptation: A theoretical treatment. *Journal of the Optical Society of America*, 58, 404–415. [PubMed]
- Naarendorp, F., Sato, Y., Cajdric, A., & Hubbard, N. P. (2001). Absolute and relative sensitivity of the scotopic system of rat: Electroretinography and behavior. *Visual Neuroscience*, 18, 641–656. [PubMed]
- Nygaard, R. W., & Frumkes, T. E. (1985). Frequency dependence in scotopic flicker sensitivity. *Vision Research*, 25, 115–127. [PubMed]
- Parinaud, H. (1881). L'héméralopie et les fonctions du pourpre visuel. *Comptes rendus hebdomadaires des séances et mémoires de la Société de biologie*, 93, 286–287.
- Penn, R. D., & Hagins, W. A. (1972). Kinetics of photocurrent of retinal rods. *Biophysical Journal*, 12, 1073–1094. [PubMed] [Article]
- Pugh, E. N., Jr. (1988). Vision: Physics and retinal physiology. In R. C. Atkinson, R. J. Herrnstein, G. Lindsey, & R. D. Luce (Eds.), *Stevens' handbook of experimental psychology, second edition* (vol. 1, pp. 75–163). New York: Wiley.
- Pugh, E. N., Jr., & Lamb, T. D. (2000). Phototransduction in vertebrate rods and cones: Molecular mechanisms of amplification, recovery and light adaptation. In D. G. Stavenga, W. J. de Grip, & E. N. Pugh (Eds.), *Handbook of biological physics, Vol. 3, Molecular mechanisms of visual transduction* (pp. 183–255). Amsterdam: Elsevier.
- Pugh, E. N., Jr., Nikonov, S., & Lamb, T. D. (1999). Molecular mechanisms of vertebrate photoreceptor light adaptation. *Current Opinion in Neurobiology*, 9, 410–418. [PubMed]
- Roufs, J. A. J. (1972a). Dynamic properties of vision: I. Experimental relationships between flicker and flash thresholds. *Vision Research*, 12, 261–278. [PubMed]
- Roufs, J. A. J. (1972b). Dynamic properties of vision: II. Theoretical relationship between flicker and flash thresholds. *Vision Research*, 12, 279–292. [PubMed]
- Rushton, W. A. H. (1965). The Ferrier lecture, 1962: Visual adaptation. *Proceedings of the Royal Society of London B: Biological Sciences*, B162, 20–46.
- Rushton, W. A. H., & Westheimer, G. (1962). The effect upon the rod threshold of bleaching neighbouring rods. *The Journal of Physiology*, 164, 318–329. [PubMed] [Article]
- Schiller, P. H., & Malpeli, J. G. (1977). Properties and tectal projections of monkey retinal ganglion cells. *Journal of Neurophysiology*, 40, 428–445. [PubMed]
- Schultze, M. (1866). Zur Anatomie und Physiologie der Retina. *Archiv für mikroskopische Anatomie und Entwicklungsmechanik*, 2, 175–286.
- Shapley, R., & Enroth-Cugell, C. (1984). Visual adaptation and retinal gain controls. In N. Osborne & G. Chader (Eds.), *Progress in retinal research* (vol. 3, pp. 263–346). New York: Pergamon Press.
- Sharpe, L. T., & Stockman, A. (1999). Rod pathways: The importance of seeing nothing. *Trends in Neurosciences*, 22, 497–504. [PubMed]
- Sharpe, L. T., Stockman, A., Fach, C. C., & Markstahler, U. (1993). Temporal and spatial summation in the human rod visual system. *The Journal of Physiology*, 463, 325–348. [PubMed] [Article]
- Sharpe, L. T., Stockman, A., & MacLeod, D. I. A. (1989). Rod flicker perception: Scotopic duality, phase lags and destructive interference. *Vision Research*, 29, 1539–1559. [PubMed]
- Smith, R. A., Jr. (1969). Quantum efficiency and the scotopic MTF. *Journal of the Optical Society of America*, 59, 1538.
- Smith, R. A., Jr. (1973). Luminance-dependent changes in mesopic visual contrast sensitivity. *The Journal of Physiology*, 230, 115–135. [PubMed] [Article]
- Sperling, G., & Sondhi, M. M. (1968). Model for visual luminance discrimination and flicker detection. *Journal of the Optical Society of America*, 58, 1133–1145. [PubMed]
- Stabell, U., Nordby, K., & Stabell, B. (1987). Light-adaptation of the human rod system. *Clinical Vision Sciences*, 2, 83–91.
- Stockman, A., Langendörfer, M., & Sharpe, L. T. (2007). Human S-cone light adaptation. *Journal of Vision*, 7(3):4, 1–7, <http://journalofvision.org/7/3/4/>, doi:10.1167/7.3.4. [PubMed] [Article]
- Stockman, A., Langendörfer, M., Smithson, H. E., & Sharpe, L. T. (2006). Human cone light adaptation: From behavioral measurements to molecular mechanisms. *Journal of Vision*, 6(11):5, 1194–1213, <http://journalofvision.org/6/11/5/>, doi:10.1167/6.11.5. [PubMed] [Article]
- Stockman, A., Sharpe, L. T., Rütger, K., & Nordby, K. (1995). Two signals in the human rod visual system: A model based on electrophysiological data. *Visual Neuroscience*, 12, 951–970. [PubMed]
- Thomas, M. M., & Lamb, T. D. (1999). Light adaptation and dark adaptation of human rod photoreceptors measured from the a-wave of the electroretinogram. *The Journal of Physiology*, 518, 479–496. [PubMed] [Article]
- Tranchina, D., Gordon, J., & Shapley, R. M. (1984). Retinal light adaptation—evidence for a feedback mechanism. *Nature*, 310, 314–316. [PubMed]
- van den Brink, G., & Bouman, M. A. (1954). Variation of integrative actions in the retinal system: An adaptational phenomenon. *Journal of the Optical Society of America*, 44, 616–620. [PubMed]

- von Kries, J. (1894). Über den Einfluß der Adaptation auf Licht- und Farbenempfindung und über die Funktion der Stäbchen. *Bericht der naturforschungs Gesellschaft, Freiburg im Breisgau*, 9, 61–70.
- von Kries, J. (1896). Über die Funktion der Netzhautstäbchen. *Zeitschrift für Psychologie und Physiologie der Sinnesorgane*, 9, 81–123.

- Watson, A. B. (1986). Temporal sensitivity. In K. Boff, L. Kaufman, & J. Thomas (Eds.), *Handbook of perception and human performance* (vol. 1, pp. 6-1–6-43). New York: Wiley.